Inorganic Chemistry
Communication

Inorg. Chem. **2009,** *48,* 4655–4657 **4655**
DOI:10.1021/ic9003802

Solid-State Coordination Chemistry of Copper(II) Tetrazolates: Anion Control of Frameworks Constructed from Trinuclear Copper(II) Building Blocks

Wayne Ouellette,[†] Hongxue Liu,[‡] Charles J. O'Connor,[‡] and Jon Zubieta*[,†]

[†]*Department of Chemistry, Syracuse University, Syracuse, New York 13244, and* [‡]*Advanced Materials Research Institute, University of New Orleans, New Orleans, Louisiana 70148*

Received March 10, 2009

The products of the reactions of copper(II) starting materials with 4-pyridyltetrazole (4-Hpt) in *N*,*N*-dimethylformamide (DMF)/methanol solutions are determined by the anion identity and concentration. In the absence of chloride, the 3-D open-framework material $[Cu_3(OH)_3(4\text{-pt})_3(DMF)_4]\cdot 5DMF\cdot 3MeOH$ (**1**·5DMF·3MeOH) is isolated, while variations in the chloride concentration yield the 2-D and 3-D materials, **2** and **3**, respectively. All three structures exhibit trinuclear copper(II) building blocks: the triangular $\{Cu_3(\mu_3\text{-OH})\}^{5+}$ core in **1** and $\{Cu_3Cl_4(4\text{-pt})_4(4\text{-Hpt})_2\}^{2-}$ and $\{Cu_3Cl_2(4\text{-pt})_8\}^{4-}$ chains in **2** and **3**, respectively. All three materials display microporosity, which is highly dependent on the method of sample preparation.

Metal−organic frameworks (MOFs) continue to receive significant contemporary attention, reflecting their applications to fields as diverse as gas storage, separation, and catalysis.[1−4] MOFs have been featured prominently in the design of zeolitic mimics, exploiting a synthetic strategy based on metal or metal cluster nodes tethered through dipodal or multipodal organic spacers.[5,6] While the majority of MOFs have been constructed from carboxylate and polypyridyl ligands,[7] polyazaheteroaromatic ligands such as imidazolate, pyrazolate, triazolate, and tetrazolate have been exploited more recently in the design of such hybrid materials.[8−11] This class of ligands affords the ability to bridge metal sites, as well as a superexchange capacity reflected in the unusual magnetic properties of their complexes.[12,13] Furthermore, polyazaheteroaromatic ligands are readily derivatized to provide bridging ligands with additional functionality.

In the course of our investigations of strategies for the construction of hybrid materials from molecular building blocks, we studied the hydrothermal chemistry of triazole with various transition-metal cations in the preparation of materials displaying sorptive, magnetic, or luminescent properties.[14] One of these materials, $[Cu_3(OH)_3(trz)_3(H_2O)_4]\cdot 4.5H_2O$ (trz = 1,2,4-triazolate), exhibited microporous character and magnetic properties consistent with spin frustration. Encouraged by these results, we sought to investigate the consequences of ligand modification to allow spatial expansion of the framework and a potential increase in the accessible void volume. The ligand 4-pyridyltetrazolate (Hpt) can be considered as an expanded analogue of 1,2,4-triazolate (Figure S24 in the Supporting Information, SI). However, while $[Cu_3(OH)_3(4\text{-pt})_3(DMF)_4]\cdot 5DMF\cdot 3MeOH$ (**1**·5DMF·3MeOH, where DMF = *N*,*N*-dimethylformamide), a material analogous to $[Cu_3(OH)_3(trz)_3(H_2O)_4]\cdot 4.5H_2O$, was obtained, the products were dependent on the identity and concentration of the anionic component of the copper starting material.[15] Thus, in the presence of different stoichiometries of chloride, $[Cu_3Cl_4(4\text{-pt})_2(4\text{-Hpt})_2]\cdot 4DMF\cdot 2MeOH$ (**2**·4DMF·2MeOH) and $[Cu_3Cl_2(4\text{-pt})_4]\cdot 4DMF\cdot 4MeOH$ (**3**·4DMF·4MeOH) were obtained.

Compound **1**·5DMF·3MeOH was prepared from the room temperature reaction of $Cu(SO_4)\cdot 5H_2O$ with 4-Hpt in the presence of dilute H_2SO_4 in a mixed DMF/methanol solution.[16] Compounds **2**·4DMF·2MeOH and **3**·4DMF·4MeOH were isolated from DMF/methanol

*To whom correspondence should be addressed. E-mail: jazubiet@syr.edu.

(1) Hagashi, H.; Côté, A. P.; Furukawa, H.; O'Keefe, M.; Yaghi, O. M. *Nat. Mater.* **2007**, *6*, 501–506.
(2) Collins, D. J.; Zhou, H.-C. *J. Mater. Chem.* **2007**, *17*, 3154–3160.
(3) Morris, R. E.; Wheatley, P. S. *Angew. Chem., Int. Ed.* **2008**, *47*, 4966–4981.
(4) Ohmori, O.; Kawano, M.; Fujita, M. *Angew. Chem., Int. Ed.* **2008**, 1994–1997.
(5) Cheetham, A. K.; Rao, C. N. R.; Feller, R. K. *Chem. Commun.* **2006**, 4780–4798.
(6) Tranchemontagne, D. J.; Ni, Z.; O'Keefe, M.; Yaghi, O. M. *Angew. Chem., Int. Ed.* **2008**, *47*, 5136–5147.
(7) Rao, C. N. R.; Natarajan, S.; Vaidhzanathan, R. *Angew. Chem., Int. Ed.* **2004**, *43*, 1466–1496.
(8) Dinca, M.; Yu, A. F.; Long, J. R. *J. Am. Chem. Soc.* **2006**, *128*, 8904–8913.
(9) Park, K. S.; Ni, Z.; Côté, A. P.; Choi, J. Y.; Huang, R.; Uribe-Romo, F. J.; Chae, H. K.; O'Keefe, M.; Yaghi, O. M. *Proc. Natl. Acad. Sci.* **2006**, *103*, 10186–10191.
(10) Zhang, J.-P.; Chen, X.-M. *Chem. Commun.* **2006**, 1689–1699.
(11) Zhao, H.; Qu, Z.-R.; Ye, H.-Y.; Xiong, R.-G. *Chem. Soc. Rev.* **2008**, *37*, 84–100.
(12) Hasnoot, J. G. *Coord. Chem. Rev.* **2000**, *200*−*202*, 135–185.
(13) Kahn, O.; Martinez, C. J. *Science* **1998**, *279*, 44–48.
(14) Ouellette, W.; Prosvirin, A. V.; Valeich, J.; Dunbar, K. R.; Zubieta, J. *Inorg. Chem.* 2007, *46*, 9067−9082 and references cited therein.
(15) Gimeno, N.; Vilar, R. *Coord. Chem. Rev.* **2006**, *250*, 3161.
(16) See the Supporting Information.

Published on Web 5/6/2009

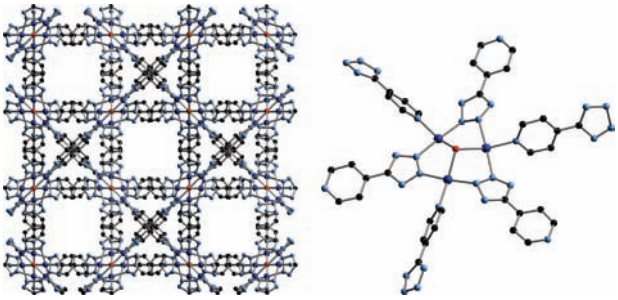

Figure 1. (a) View of the framework structure of **1**·5DMF·3MeOH in the *ab* plane. (b) Trinuclear building block of **1**·5DMF·3MeOH. Color scheme: copper, blue spheres; oxygen, red spheres; nitrogen, light-blue spheres; carbon, black spheres. This scheme is used throughout.

solutions with different chloride stoichiometries. The thermogravimetric analysis (TGA) profile of **1**·5DMF·3MeOH exhibited a rapid weight loss starting at room temperature to 150 °C of 31%, corresponding to the loss of the DMF and methanol of crystallization. This desolvation process was followed by ligand decomposition and the loss of coordinated DMF in the 160−290 °C range. Consequently, the material exhibited no plateau of stability in its TGA profile (Figure S3 in the SI). On the other hand, when **1**·5DMF·3MeOH was soaked in methanol overnight, the solvent DMF was displaced to provide **1**·12MeOH, as confirmed by elemental analysis and TGA (see the SI). In this case, the solvent was cleanly removed between room temperature and 70 °C, providing a plateau of stability for the desolvated **1** from 70 to 220 °C. The powder X-ray diffraction (XRD) profiles of **1**·5DMF·3MeOH and desolvated **1**·12MeOH indicate that no significant structural changes occur as a result of the thermal process (Figure S1 in the SI), while the IR spectra clearly show the loss of the DMF of crystallization (Figure S2 in the SI).[18] Similar behavior was observed for compounds **2** and **3**, such that soaking in methanol displaced the DMF of crystallization and provided methanol solvates with improved TGA profiles (Figures S8−S10 and S14−S16 in the SI).

As shown in Figure 1a, the structure of **1**·5DMF·3MeOH consists of a 3-D MOF encompassing a considerable solvent-accessible volume.[17] The framework is constructed from the linking of trinuclear $\{Cu_3(\mu_3\text{-OH})\ (4\text{-pt})_3(OH)_2(DMF)_4\}$ building blocks (Figure 1b) through the exocyclic pyridyl N atom, in a manner reminiscent of the structure of $[Cu_3(OH)_3(trz)_3(H_2O)_4]\cdot 4.5H_2O$. The "4 + 2" axially distorted geometry at each Cu^{II} site is defined by two N donors from the 4-pt groups in the cluster, the μ_3-OH group, and a pyridyl N atom from the 4-pt ligand of an adjacent trinuclear cluster in the equatorial plane and either two DMF ligands or a DMF ligand and a hydroxy group in the axial positions. Each trinuclear subunit is linked to six

(17) Crystal data for **1**·5DMF·3MeOH: $C_{48}H_{90}Cu_3N_{24}O_{15}$, fw 1434.06, cubic $Fd\bar{3}c$, a = 36.0387(6) Å, V = 46806.6(13) Å^3, Z = 32, D_{calcd} = 1.628 g/cm^3, μ(Mo Kα) = 11.69 cm^{-1}, R1 = 0.0965, wR2 = 0.2235 (1635 reflections). Crystal data for **2**·4DMF·2MeOH: $C_{19}H_{27}Cl_2Cu_{1.5}N_{12}O_3$, fw 637.74, monoclinic $P2_1/c$, a = 11.1039(6) Å, b = 11.3999(6) Å, c = 21.9492(11) Å, β = 104.620(1)°, V = 2688.4(2) Å^3, Z = 4, D_{calcd} = 1.576 g/cm^3, μ(Mo Kα) = 14.42 cm^{-1}, R1 = 0.0594, wR2 = 0.0913 (6522 reflections). Crystal data for **3**·4DMF·4MeOH: $C_{40}H_{60}Cl_2Cu_3N_{24}O_8$, fw 1266.64, orthorhombic $Pnnm$, a = 12.0495(11) Å, b = 14.8817(13) Å, c = 15.9221(14) Å, Z = 2, V = 1.473 g/cm^3, D_{calcd} = 1.473 g/cm^3, μ(Mo Kα) = 12.70 cm^{-1}, R1 = 0.1279, wR2 = 0.2198 (3523 reflections).

(18) Rajagopal, S.; Vancheesan, S.; Rajaram, J.; Kuriccose, J. C. *J. Mol. Catal.* **1983**, *22*, 131–135.

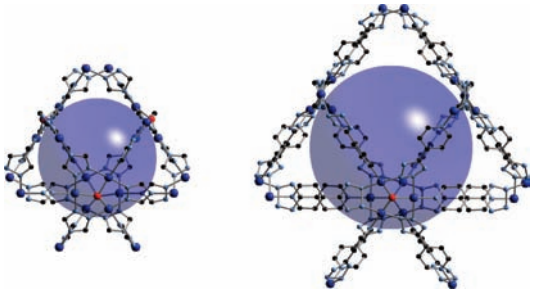

Figure 2. Comparison of the relative pore dimensions of $[Cu_3(OH)_3(trz)_3(H_2O)_4]$ (left) and **1**·5DMF·3MeOH (right).

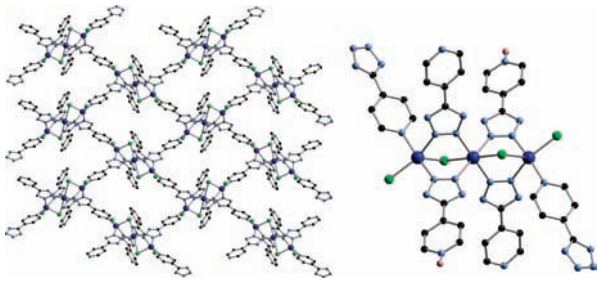

Figure 3. (a) 2-D network structure of $[Cu_3Cl_4(4\text{-pt})_2(4\text{-Hpt})_2]\cdot 4DMF\cdot 2MeOH$ (**2**·4DMF·2MeOH) in the *bc* plane. (b) $\{Cu_3Cl_4(4\text{-pt})_4(4\text{-Hpt})_2\}^{2-}$ building unit of **2**. The color scheme is the same as that for Figure 1 with green spheres for chlorine and pink spheres for hydrogen.

adjacent clusters to generate a framework exhibiting 68% accessible void volume. As shown in Figure 2, the connectivity pattern generates cages of 18.0-Å diameter with communicating windows of dimensions 9.5 Å × 9.5 Å. In contrast, the cages associated with the structure of $[Cu_3(OH)_3(trz)_3(H_2O)_4]\cdot 4.5H_2O$ exhibit a diameter of 12.0 Å and windows of 3.5 Å × 3.5 Å.

The structure of the first chloride derivative **2**·4DMF·2MeOH is 2-D as shown in Figure 3a. The structure is constructed from trinuclear $\{Cu_3Cl_4(4\text{-pt})_4(4\text{-Hpt})_2\}^{2-}$ chains, illustrated in Figure 3b. The Cu^{II} sites at the termini exhibit distorted "4 + 1" square-pyramidal geometries $\{CuCl_2N_3\}$ defined by a μ_2-Cl in the apical position and a terminal Cl, two N donors from two bridging tetrazolate groups, and a pyridyl donor from a third 4-pt ligand in the basal plane. The central Cu site exhibits "4 + 2" six-coordination with two bridging Cl atoms in the axial positions and four N donors from bridging tetrazolate ligands defining the equatorial plane. Each trinuclear cluster is linked to four adjacent clusters in the layer through the two 4-pt ligands on the terminal Cu sites and two of the four bridging ligands. The two remaining pyridyltetrazole groups associated with the cluster subunit are protonated at the pyridyl N atoms and project into the interlamellar domain. These projecting groups serve to sculpt the interlamellar region and to provide a structural profile reminiscent of "pillared" layer materials. Hydrogen bonding between the protonated pyridyl N atom and the adjacent $\{Cu_3Cl_4(pt)_2\}_n$ layers results in a virtual framework structure that can sorb various guest molecules (vide infra).

When the Cu/Cl stoichiometry is lowered, the 3-D material **3**·4DMF·4MeOH is obtained (Figure 4a). The building block is once again a trinuclear chain, $\{Cu_3Cl_2(4\text{-pt})_8\}^{4-}$ as shown in Figure 4b. This subunit is similar to that of **2**·4DMF·2MeOH with the terminal C atoms replaced by the pyridyl N donors of two 4-pt ligands. Because there is no

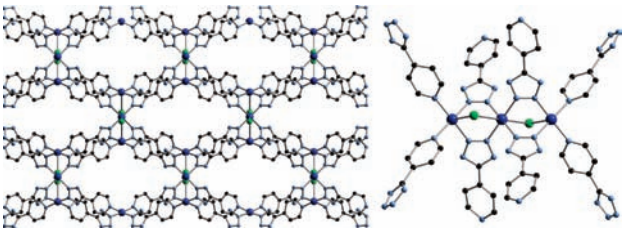

Figure 4. (a) Framework structure of **3**·4MDF·4MeOH, viewed in the *bc* plane. (b) $\{Cu_3Cl_2(4\text{-pt})_8\}^{4-}$ building unit of **3**.

protonation of pyridyl N atoms for **3**·4DMF·4MeOH, each 4-pt ligand spans two adjacent trinuclear clusters; consequently, each cluster is linked to eight neighboring clusters to generate the 3-D connectivity.

The TGA characteristics of **1**−**3** suggested that the sorptive properties of these open-framework materials would be significantly influenced by the desolvation procedures. This observation was confirmed in all cases. Thus, compound **1**·5DMF·3MeOH was soaked in H_2O at 80 °C to provide $[Cu_3(OH)_3(pt)_3(H_2O)_4]\cdot xH_2O$ (**1a**).[15] Compound **1a** was heated to 50 °C under vacuum to provide the desolvated material **1′** (Figures S1 and S2 in the SI). As shown in Figure 5, sample treatment has a pronounced effect on the N_2 sorption isotherms. Thus, desolvated samples of **1**·5DMF·3MeOH provide Brunauer−Emmett−Teller (BET) and Langmuir surface areas of 559 and 587 m^2/g, respectively, while those of **1′** give BET and Langmuir surface areas of 1243 and 1317 m^2/g, respectively. This observation may reflect the displacement of the coordinated DMF molecules with the sterically less demanding aqua ligands. This effect is also apparent in the Horvath−Kawazoe differential pore-volume plots for **1**·5DMF·3MeOH and **1′**, which give pore widths of 13.1 and 15.3 Å, respectively (Figures S5−S7 in the SI). Similarly, the H_2 sorption curves for **1**·5DMF·3MeOH and **1′** exhibit 0.90 and 1.76 wt % sorption, respectively. While desolvated samples of **2**·4DMF·2MeOH and **3**·4DMF·3MeOH exhibit negligible surface areas, the methanol-soaked and desolvated **2** and **3** exhibit BET surface areas of 389 and 380 m^2/g with weight percent uptake of H_2 of 0.75 and 0.73 wt %, respectively (Figures S11, S12, S17, and S18 in the SI).

The compounds **1**−**3** exhibit a range of magnetic properties. Thus, the magnetism of **1** conforms to a trimer equilateral triangle model (Figure S7 in the SI). However, the coupling constants J/K and zJ'/K of −27.5 and −0.23 cm^{-1},[15] respectively, are significantly smaller than those observed for the structurally analogous $[Cu_3(OH)_3(trz)_3(H_2O)_4]\cdot 4H_2O$ (**4**). While the $\{Cu_3(\mu_3\text{-}OH)\}$ unit and the triazolate ligands of **4** are coplanar, maximizing the superexchange capacity of the polyazaheterocycle, the tetrazolate planes of **1** are distinctly out of the $\{Cu_3(OH)\}$ plane with an interplanar angle of 18.0° (Figure S23 in the SI). Likewise, while the magnetism of **3** (Figure S19 in the SI) conforms to a linear trimer,[15] the J and zJ' values of −3.51 and 0.57 cm^{-1}, respectively, are significantly less negative than those reported for the

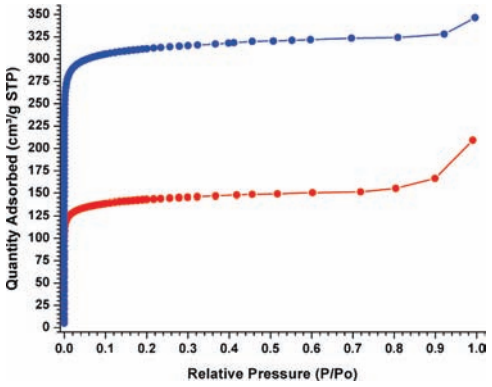

Figure 5. N_2 sorption isotherms for desolvated **1**·5DMF·3MeOH (red) and **1′** (blue).

analogous linear trimer in $[Cu_3(trz)_4(H_2O)_3]F_2$ (**5**)[14] (−130 and −51 cm^{-1}). Once again, the magnetic orbitals in **5** ($d_{x^2-y^2}$) are coplanar, while those of **3** exhibit an interplanar angle of 106.4° at the central Cu^{II} site, resulting in poor overlap and concomitant decreased efficiency of superexchange through the ligand. This effect is even more pronounced in **2**, where distortion of the terminal Cu^{II} sites toward trigonal-bipyramidal geometry renders the overlap of magnetic orbitals negligible. The magnetism of **2** can be modeled in terms of three noninteracting Cu^{II} ions obeying the Curie−Weiss law (Figure S13 in the SI).[16]

In conclusion, the Hpt ligand is effective in bridging metal sites to provide open-framework materials. A recurring theme of the structures is the presence of trinuclear clusters as secondary building blocks. However, the identity of the building units and the details of their overall connectivity in the construction of the solids are dependent on the anionic components and concentrations. Furthermore, actualizing the microporosity of these materials requires careful sample preparation because rapid removal of the DMF of crystallization results in poor sorptive properties, presumably because of partial collapse of the framework structure. In the case of **1**, the displacement of coordinated DMF by aqua ligands results in considerable surface area and modest H_2 sorption. The magnetic properties of the materials are quite distinct from those of the copper(II) triazolate family, most likely because of geometric factors that minimize superexchange through the tetrazole moiety.

Acknowledgment. This work was funded by a grant from the National Science Foundation (Grant CHE-0604527).

Supporting Information Available: Description of experimental details, including synthetic methods, crystallography, magnetism, and sorption; supplementary figures, including TGA, IR spectroscopy, powder XRD profiles, gas sorption isotherms, and anisotropic thermal ellipsoids for compounds **1**−**3**; Tables of crystallographic data and CIF files for compounds **1**−**3**. This material is available free of charge via the Internet at http://pubs.acs.org.